JACS
JOURNAL OF THE AMERICAN CHEMICAL SOCIETY

Article

pubs.acs.org/JACS

Biological Photothermal Nanodots Based on Self-Assembly of Peptide–Porphyrin Conjugates for Antitumor Therapy

Qianli Zou,[†,#] Manzar Abbas,[†,§,#] Luyang Zhao,[†] Shukun Li,[†,§] Guizhi Shen,[†] and Xuehai Yan*[,†,‡]

[†]State Key Laboratory of Biochemical Engineering, Institute of Process Engineering, Chinese Academy of Sciences, Beijing 100190, China

[‡]Center for Mesoscience, Institute of Process Engineering, Chinese Academy of Sciences, Beijing 100190, China

[§]University of Chinese Academy of Sciences, Beijing 100049, China

Supporting Information

ABSTRACT: Photothermal agents can harvest light energy and convert it into heat, offering a targeted and remote-controlled way to destroy carcinomatous cells and tissues. Inspired by the biological organization of polypeptides and porphyrins in living systems, here we have developed a supramolecular strategy to fabricate photothermal nanodots through peptide-modulated self-assembly of photoactive porphyrins. The self-assembling nature of porphyrins induces the formation of J-aggregates as substructures of the nanodots, and thus enables the fabrication of nanodots with totally inhibited fluorescence emission and singlet oxygen production, leading to a high light-to-heat conversion efficiency of the nanodots. The peptide moieties not only provide aqueous stability for the nanodots through hydrophilic interactions, but also provide a spatial barrier between porphyrin groups to inhibit the further growth of nanodots through the strong π-stacking interactions. Thermographic imaging reveals that the conversion of light to heat based on the nanodots is efficient in vitro and in vivo, enabling the nanodots to be applied for photothermal acoustic imaging and antitumor therapy. Antitumor therapy results show that these nanodots are highly biocompatible photothermal agents for tumor ablation, demonstrating the feasibility of using bioinspired nanostructures of self-assembling biomaterials for biomedical photoactive applications.

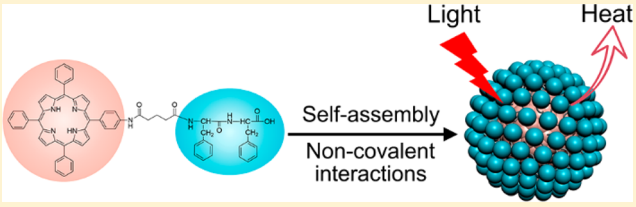

INTRODUCTION

Photothermal therapy (PTT) is a promising and elegant therapeutic means against tumors due to inherent advantages of minimum invasiveness, easy procedure, short treatment time, and quick recovery.[1] PTT greatly depends on use of photothermal agents that are essential to efficiently convert light energy into heat for thermal ablation of cancer cells and tumors.[2] Photothermal agents also serve as contrast agents for the emerging diagnostic technique of photoacoustic (PA) imaging,[3,4] which provides deeper penetration in biological tissue and higher resolution than traditional optical imaging techniques.[5−7] For a long time, therefore, people have been dedicated to the development of new types of photothermal materials and agents to meet the increasing demands of photothermal therapeutics and diagnostics in clinic applications.[8]

So far, a variety of photoactive nanomaterials, such as gold nanoparticles and nanorods,[9−11] graphenes and graphene oxide,[12,13] black phosphorus quantum dots and nanosheets,[14,15] and light-absorbing polymer (e.g., polypyrole) nanoparticles,[16,17] have been developed as photothermal agents for tumor PA imaging and PTT. However, inorganic photothermal materials are suffering from long-term biosafety due to their non-bioderivative and non-biodegradable features, limiting their further clinical applications. Although polymer nanoparticles are emerging for overcoming the shortcomings of inorganic photothermal materials, a majority of them are still subject to a lot of limitations concerning complicated fabrication processes, indistinct biodegradation, and potential biosafety. As an alternative and innovative strategy, simple biomolecules of biological origin provide answers for addressing the above-mentioned issues in design of photothermal materials. For example, Zheng et al. developed phorphyrin-incorporated lipid bilayer nanovesicles with photothermal response based on self-assembly of porphyrin-coupled lipids, showing a therapeutic potential.[18] However, lipid bilayers are generally considered unstable, susceptible to disassembly and decomposition both in blood circulation and in storage.[19] Therefore, it still remains a formidable challenge to design and create photothermal nanomaterials starting from small biomolecule combinations and their cooperative interactions.

In living mammalian tissues, light-absorbing hemoglobin is found being an endogenous photothermal macromolecule formed by cooperative interactions of porphyrins and proteins.[20] Inspired by the natural protein-based photothermal species, herein we put forward a strategy of peptide-modulated self-assembly of photoactive dyes such as porphyrins for design and engineering of photothermal nanoparticles toward antitumor therapy. Short peptides, consisting of several amino

Received: November 2, 2016
Published: January 19, 2017

DOI: 10.1021/jacs.6b11382
J. Am. Chem. Soc. 2017, 139, 1921−1927

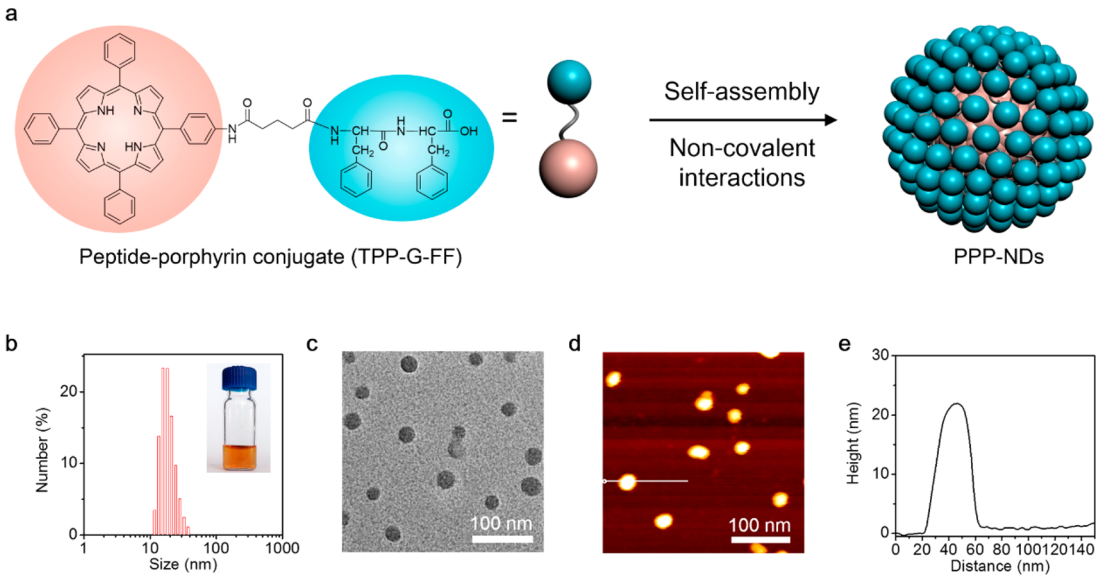

Figure 1. Self-assembly of a peptide−porphyrin conjugate (TPP-G-FF) into photothermal peptide−porphyrin nanodots (PPP-NDs). (a) Molecular structure of TPP-G-FF and schematic illustration of the self-assembly. (b) DLS size distribution of PPP-NDs. The inset is a picture of PPP-NDs in water at the concentration of 0.2 mg mL^{-1}. (c) TEM image of PPP-NDs. (d,e) AFM topography image of PPP-NDs on mica substrate and height profile along the line in single ND, indicating 23 nm in its height.

acids, are of particular interest as a regulator for creation of biomimetic systems and advanced materials,[21−23] owing to inherent biological origin, structural programmability, excellent biocompatibility and biodegradability, low immunogenicity, and versatile functionality as well as high availability.[24−28] We for the first time achieve the fabrication of photothermal nanodots of around 25 nm diameter with long-term colloidal stability by tuning the molecular interactions of the peptide−porphyrin conjugates (Figure 1a). Strong π-stacking in the assembled nanodots leads to the complete quenching of fluorescence and inhibition of generating reactive oxygen species, ultimately obtaining a highly efficient light-to-heat energy conversion. Electrostatic repulsion of the negatively charged surface of nanodots maintains a long-term colloidal storage stability and blood circulation stability. The assembled peptide−porphyrin photothermal nanodots (PPP-NDs) reveal high tumor accumulation, negligible toxicity, and effective tumor ablation. Taken together, our results demonstrate a new supramolecular strategy for rational design and construction of highly stable and efficient photothermal nanoparticles toward antitumor therapy based on the combination of biological light-absorbing molecules and self-assembling peptides.

RESULTS AND DISCUSSION

L-Phenylalanine-L-phenylalanine (FF) is the core self-assembling motif extracted from Alzheimer's β-amyloid polypeptide.[29] FF assemblies have proven to exhibit remarkable advantages, including ease of production, functional versatility, biodegradability, biocompatibility, and non-immunogenicity.[30−33] Also, we demonstrate tunable co-assembly of FF with various functional molecules through non-covalent interactions is a versatile approach to obtain nanomaterials with controllable morphology and considerable stability.[34,35] Hence, FF was selected as the key moiety of the self-assembling peptide−porphyrin conjugate. The synthesized peptide−porphyrin conjugate (TPP-G-FF) undergoes self-assembly for formation of well-defined nanodots with flexibly controlled size ranging from 20 to 100 nm upon dissolution in dimethyl sulfoxide (DMSO) and then dilution with pure water, depending on the initial concentration (see Figure S6 in the Supporting Information). Dynamic light scattering (DLS) profiles reveal that the size of PPP-NDs prepared at the concentration of 0.2 mg mL^{-1} is 25 ± 10 nm (Figure 1b). It is well-known that small nanomaterials in the range from approximately 10 to 100 nm are highly preferred for biomedical applications, because they can passively accumulate in tumors through the enhanced permeability and retention (EPR) effect.[36] PPP-NDs with size of 25 ± 10 nm in diameter were used for further characterization and biomedical application. Transmission electron microscopy (TEM) images disclose that PPP-NDs are in a regular spherical shape with a size of average 28 nm, almost consistent with the DLS result (Figure 1c). Atomic force microscopy (AFM) images also confirm that these nanodots are spherical and have a uniform size distribution (Figure 1d,e). The zeta potential of PPP-NDs (−23 ± 3.2 mV) explains, why the dispersion of nanodots is a stable and biocompatible colloidal system.

Subsequently, the mechanisms behind the self-assembly process were investigated. A bathochromic shift and a broadening were found for Soret and Q bands in the absorption spectra of PPP-NDs as compared with those of TPP-G-FF (Figure 2), indicating that π-stacking of tetraphenylporphyrin (TPP) is contributing to the formation of PPP-NDs as well as the hydrophobic effect.[37] A molecular dynamics (MD) simulation of a simplified model that contains six TPP-G-FF molecules in a water box sized 6.0 × 6.0 × 6.0 nm^3 showed that all six TPP-G-FF molecules quickly self-assembled with the time (Figure 3). The corresponding structures show that the TPP moieties are apt to form J-aggregates, in which the distances between two TPP moieties are 3.6−4.2 Å, and the average energy due to the π-stacking is around −27 kcal mol^{-1} for each interaction pair, indicating strong hydrophobic effects. In addition, the FF chains are either stretched into the solvent due to its hydrophilicity or stacked with TPP by the π-stacking between the phenyl moiety and TPP, reasonably because FF is an amphiphilic moiety. In terms of the hydrophilic effect, there

DOI: 10.1021/jacs.6b11382
J. Am. Chem. Soc. 2017, 139, 1921−1927

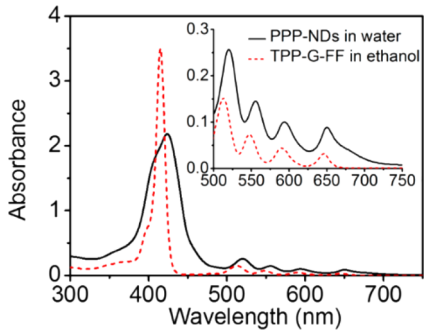

Figure 2. UV−vis absorption spectra of PPP-NDs in water and TPP-G-FF in ethanol. The inset shows magnified absorption spectra of Q-bands.

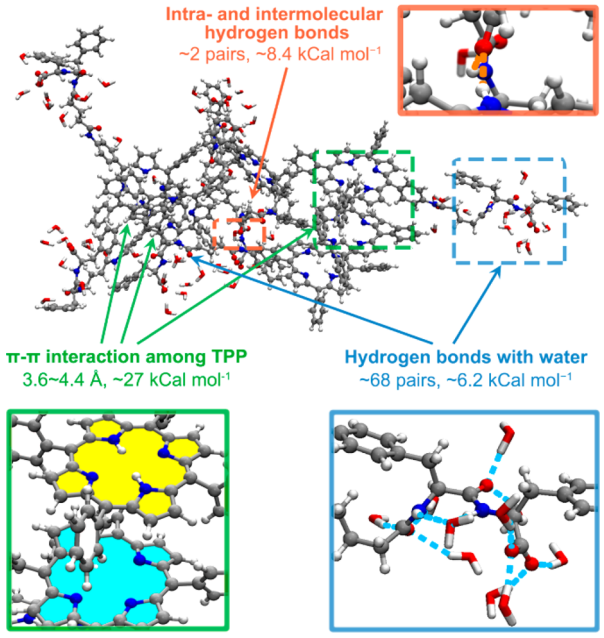

Figure 3. Structures of the self-assembled system containing six TPP-G-FF molecules, obtained by MD simulation. The key positions of non-covalent interactions are pointed out by arrows with the distance between the interacting moieties, numbers of pairs, and the average energy of each pair of interaction. Water molecules that have hydrophilic interactions with TPP-G-FF, are also shown. The magnified graphs show representative structures, displaying $\pi-\pi$ interactions, hydrogen bonds with water, and intra- and intermolecular hydrogen bonds between TPP-G-FF molecules.

were ~68 hydrophilic interaction pairs between FF moiety and solvent, and the average energy of each interaction pair is ~6.3 kcal mol^{-1}, which contribute a lot to the stability of PPP-NDs in water. In contrast, hydrogen bonds among TPP-G-FF molecules are found to be only two pairs (one intramolecular and one intermolecular bond) during the simulation process and the average energy for each pair is ~8.4 kcal mol^{-1}. Therefore, the π-stacking and hydrophilic interaction are the major driving forces for the self-assembly of the conjugate in water.

We further monitored the self-assembly process of PPP-NDs by DLS. The size profiles showed a time-dependent growth pattern in the formation process of PPP-NDs (Figure S7). At 1 min after the addition of water, the main peak of the formed nanodots is located at 5.8 nm with only a small fraction of nanodots located at 16 nm. Then the nanodots grew quickly with the increase of aging time and reached the stable size at 1 h, suggesting that the formation of PPP-NDs follows a pathway of self-assembly-induced nucleation and growth. Initially, TPP-G-FF molecules aggregate to form molecular clusters through mutual diffusion of DMSO and water. Then the clusters continue to grow mainly under the effect of π-stackings. Finally, the nanodots reach a stable state when the surface hydrophilic interaction (mainly electrostatic repulsion) between FF moiety and water is sufficient to support the existence of individual nanodots.

For biomedical applications, the stability of nanomaterials is one of the key factors.[38] Significantly, PPP-NDs are stable in water and their size is unaltered when kept in dark for six months (Figure 4a). Such a long-term stability confirms that

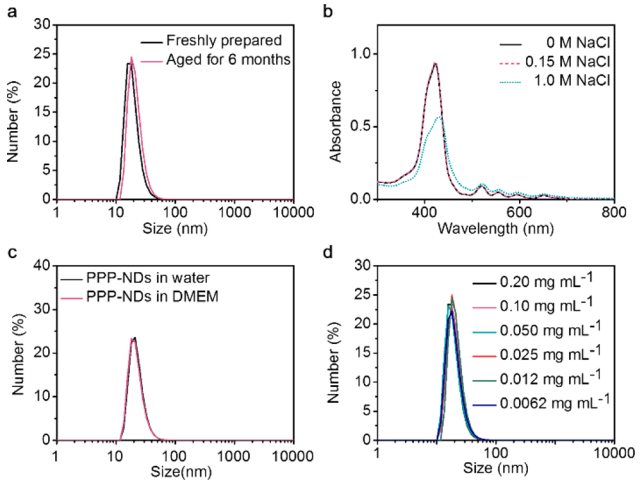

Figure 4. Stability of PPP-NDs. (a) DLS size profiles of freshly prepared and aged PPP-NDs. (b) UV−vis absorption spectra of PPP-NDs in aqueous solutions containing NaCl. (c) DLS size profiles of PPP-NDs in water and in DMEM. Before the characterization, PPP-NDs in DMEM were incubated at 37 °C for 24 h. (d) DLS size profiles for various concentrations of PPP-NDs, which were prepared at the concentration of 0.20 mg mL^{-1}, diluted to various concentrations by water, and aged for 24 h before characterization, showing the stability of PPP-NDs under dilution.

PPP-NDs are self-assembled stable colloidal nanodots other than irregular porphyrin aggregates,[39] which are prone to quickly grow into larger agglomerates due to Ostwald ripening.[40] Moreover, UV−vis absorption spectra of PPP-NDs in solution containing a physiological concentration of NaCl (0.15 M) are the same as that in water (Figure 4b). A further bathochromic shift in the absorption spectra of PPP-NDs in the presence of 1.0 M NaCl suggests that electrostatic repulsion contributes to the stability of PPP-NDs in aqueous solution. We also prepared nanoparticles of a compound containing only TPP and glutaric acid by using the same protocol for PPP-NDs. But the formed nanoparticles were unstable and completely precipitated as large agglomerates after aging for 1 day (Figure S8), suggesting that FF is essential for formation of stable PPP-NDs. FF coupling to the porphyrin could lead to a spatial barrier between porphyrin groups to inhibit the further growth of nanodots through the strong π-stacking interactions. Next, the stability of PPP-NDs in cell culture media (Dulbecco's Modified Eagle Medium, DMEM) was evaluated. When PPP-NDs were incubated in DMEM at 37 °C for 24 h, no significant change was found for their DLS

DOI: 10.1021/jacs.6b11382
J. Am. Chem. Soc. 2017, 139, 1921−1927

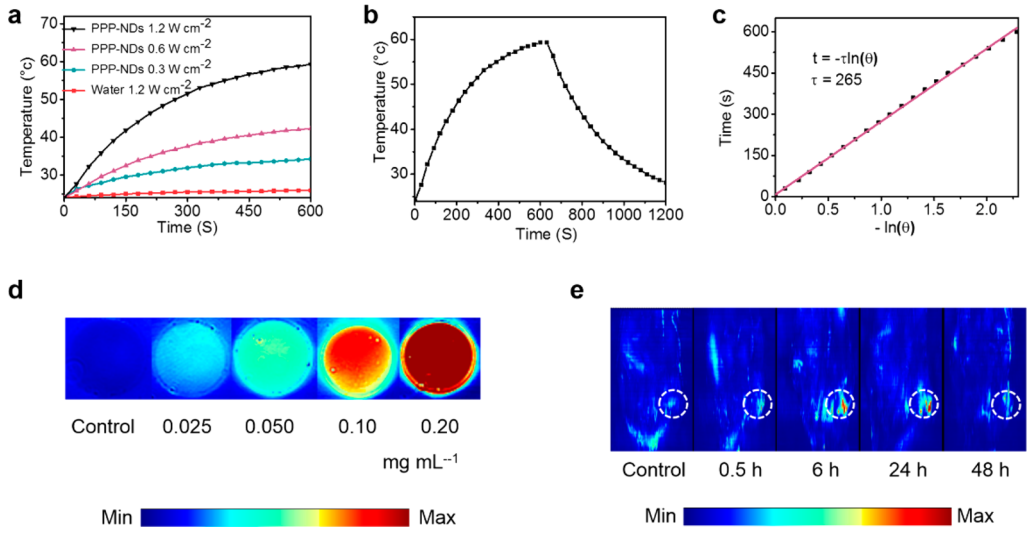

Figure 5. Photothermal and photoacoustic properties of PPP-NDs. (a) Temperature elevation for PPP-NDs in water in dependence of light intensity. (b) Photothermal effect of PPP-NDs in water when irradiated with a 635 nm laser (1.2 W cm^{-2}). The laser was switched off after irradiation for 10 min. (c) Graph of the cooling period of the time versus negative natural logarithm of the temperature. (d) PA images of PPP-NDs in water at various concentrations. Pure water was applied as a control group. (e) PA images of mice at various time points after intravenous injection of PPP-NDs. The circles indicate the tumors.

profiles (Figure 4c). Finally, the size distribution for various concentrations of PPP-NDs prepared by dilution from the same sample was tested. The DLS results showed no obvious changes in their size (Figure 4d). The high physiological stability of PPP-NDs indicates that these nanodots are promising for in vivo biomedical applications.

To demonstrate the capacity of PPP-NDs for photothermal applications we measured their photophysical properties. The light energy absorbed by a photoactive agent is normally released by four pathways: emission of photons, photochemistry, transfer to other molecules, and generation of heat.[8] According to the fluorescence spectra of PPP-NDs in water and TPP-G-FF in ethanol, a quenching yield higher than 99% is obtained for the fluorescence of PPP-NDs (Figure S9). By using tetraphenylporphine sulfonate (TPPS) as a reference,[41] the fluorescence quantum yields of TPP-G-FF and PPP-NDs are calculated to be 0.062 and 0, respectively. As the absorbed energy is transferred to adjacent molecular oxygen, reactive oxygen species such as singlet oxygen could be generated.[42] Since singlet oxygen has a characteristic phosphorescence emission band at 1270 nm,[43] we monitored the emission at 1270 nm when irradiating PPP-NDs and TPP-G-FF by using TPPS as a reference (Figure S10).[41] The emission spectra revealed that the singlet oxygen quantum yield of PPP-NDs is 0. Compared with the emission spectra of TPP-G-FF, a quenching yield higher than 99% is obtained. The suppression of both florescence and singlet oxygen is consistent with the strong π-stacking interactions in the assembled nanodots, which provides an extremely high potency for PPP-NDs as a photothermal agent. To directly evaluate the photothermal properties of PPP-NDs, we further measured the thermal behavior of PPP-NDs under continuous exposure of a laser by using pure water as control. After 10 min irradiation at 1.2 W cm^{-2}, the temperature of pure water only increased by 1.9 °C while the temperature of PPP-NDs increased by 35.3 °C (Figures 5a and S11). This suggests that PPP-NDs can convert light energy into heat in an effective and quick way. To determine the photothermal efficiency of PPP-NDs, the heating and cooling curve of a solution of PPP-NDs was measured (Figure 5b). According to the obtained data (Figure 5c) and a reported method,[44] the light-to-heat conversion efficiency was calculated to be 54.2%, which is higher than the values reported for other organic photothermal agents.[17] Significantly, this photothermal efficiency is also comparable with that of inorganic nanomaterials, such as copper selenide nanocrystals (22%), commercial Au nanoshells (13%) and nanorods (21%), and black phosphorus quantum dots (28.4%).[14,45] Moreover, the absorption spectra of PPP-NDs are almost the same as those of freshly prepared ones even after 1 h irradiation (Figure S12). Both the high light-to-heat conversion efficiency and the outstanding photostability suggest that PPP-NDs are promising for photothermal applications of PA imaging and PTT.

As an emerging imaging modality, PA imaging enables multiscale high-resolution imaging of biological structures.[46] We subsequently studied the feasibility of using PPP-NDs as a PA contrast agent. The PA signals obtained from an agarose gel phantom having PPP-NDs increase with concentration (Figures 5d and S13), consistent with other reported photothermal agents.[47] We further investigated in vivo PA imaging by a MCF-7 tumor model. Tumor-bearing mice were injected with PPP-NDs through the tail vein and then detected by PA imaging at various time points after injection. The PA images indicate that PPP-NDs accumulate near the tumor through passive targeting in a time-dependent manner (Figure 5e). The mean PA intensities in a region of interest illustrate that the accumulation of PPP-NDs reaches a maximum at 24 h post-injection (Figure S14), indicating a long in vivo circulation time of PPP-NDs.

The blood circulation and biodistribution of PPP-NDs were also examined by measuring the concentration of PPP-NDs in blood, organs, and tumors at different time points after the intravenous injection of PPP-NDs. The blood circulation curve shows that the pharmacokinetics of PPP-NDs follow a two-compartment model (Figure 6a). The two blood circulation half-lives are 0.22 and 16 h, respectively, indicating that PPP-NDs have a prolonged blood circulation after the initial rapid decay. Tissue distribution studies show that PPP-NDs are mainly taken up by liver and spleen (Figure 6b), probably

DOI: 10.1021/jacs.6b11382
J. Am. Chem. Soc. 2017, 139, 1921−1927

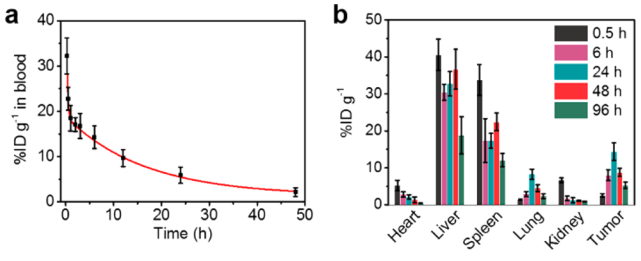

Figure 6. Blood circulation and biodistribution of PPP-NDs. (a) Concentration of PPP-NDs in blood at different time points after intravenous injection of PPP-NDs. (b) Concentration of PPP-NDs in organs and tumors at different time points after intravenous injection of PPP-NDs. Error bars represent standard deviation (n = 3).

through the mononuclear phagocyte system. At the post-injection of 96 h, the concentrations of PPP-NDs in all organs are much lower than the maximal values, indicating that PPP-NDs can be gradually cleared from the body. Recently, photothermal nanospheres constructed by integration of biodegradable polymers with black phosphorus quantum dots have shown good biodegradability and biocompatibility.[48] As compared to such organic−inorganic hybrid nanomaterials, PPP-NDs may have better biodegradability and biocompatibility due to their biologically originated nature. Significantly, the accumulation of PPP-NDs to tumors is also demonstrated by the distribution profiles. The tumor accumulation reaches a maximum of 14.3% ID g^{-1} (ID stands for injected dosage) at 24 h after the injection, consisting with the data obtained from in vivo PA imaging.

For PTT evaluation, we first analyzed the in vitro PTT efficacy and cytotoxicity of PPP-NDs in MCF-7 cells (Figure 7). Incubation of MCF-7 cells with PPP-NDs at a maximum

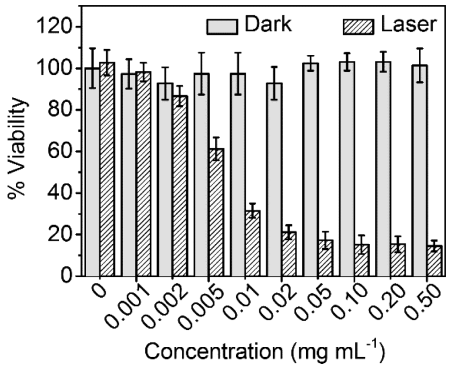

Figure 7. Viability of MCF-7 cells incubated with increasing concentration of PPP-NDs (0−0.50 mg mL^{-1}) under dark and irradiation. The cells in the laser groups were irradiated at 635 nm with an intensity of 0.3 W cm^{-2} for 10 min. Error bars represent standard deviation (n = 5).

concentration of 0.50 mg mL^{-1} in dark does not trigger discernible cytotoxicity, suggesting that PPP-NDs are highly biocompatible to cells. Under irradiation for 10 min (635 nm, 0.3 W cm^{-2}) the viability of cells decreases with the increase of PPP-ND concentration and the IC50 value is 0.0065 mg mL^{-1}. When we imaged the MCF-7 cells incubated with 0.020 mg mL^{-1} of PPP-NDs for various times, no significant fluorescence was observed after 24 h (Figure S15). Even at a prolonged incubation time of 48 h, only weak fluorescence was observed. Since TPP-G-FF is fluorescent but PPP-NDs are not, the weak in vitro fluorescence suggests that the disassembly of PPP-NDs to TPP-G-FF inside cells is slow. The disassembly of PPP-NDs to TPP-G-FF was further investigated in aqueous solution containing 0.1% Tween 80. Only 17.3% of TPP-G-FF was released from PPP-NDs at the incubation time of 48 h (Figure S16). The low disassembly rate of PPP-NDs to TPP-G-FF confirms that PPP-NDs are highly stable and robust.

To evaluate the in vivo PTT efficacy of PPP-NDs on tumors, tumor-bearing mice were divided into four groups as follows: untreated mice, mice with only PPP-ND administration (8.4 mg kg^{-1}), mice with only laser irradiation, and mice with both PPP-ND administration and laser irradiation. For irradiation, tumors were irradiated with a laser (0.3 W) for 10 min at 24 h post-injection. An IR thermal mapping camera was used to monitor the photothermal conversion under irradiation. For mice injected with PPP-NDs, the mean temperature at the tumor sites increased to 58.1 °C under irradiation for 10 min (Figure 8a,b). In comparison, the mean temperature of the tumors treated with only irradiation increased to 39.6 °C under the same irradiation (Figure S17), demonstrating that PPP-NDs are efficient for in vivo photothermal conversion. The tumors treated with both PPP-NDs and irradiation were successfully ablated, leaving dark burned scar at their original sites, while the tumors treated with only irradiation showed no significant change (Figure S18). After the treatment, the tumor volumes of mice in all groups were further monitored (Figure 8c). During 24 days of observation, no tumor recurrence was observed for mice treated with both PPP-NDs and irradiation. For mice treated with only PPP-NDs or irradiation, their tumor continued to grow rapidly, and no significant difference was found for their tumor volumes as compared with those of the untreated mice. Moreover, the body weights of mice were not significantly affected by various treatments (Figure 8d), suggesting that the PTT treatment by PPP-NDs is biocompatible. To further examine the biocompatibility of the treatment, the inside organs, including heart, spleen, kidney, liver, and lung were harvested at the end of the observation. Hematoxylin and eosin (H&E) sections of the organs from the mice treated with PPP-NDs and irradiation show no obvious pathological change or any other adverse effect as compared with the untreated group (Figure 8e). Other groups treated with only PPP-NDs or irradiation also showed no tissue damage (Figure S19). These results confirm that PTT by PPP-NDs is an efficient and biocompatible treatment for tumor ablation.

CONCLUSION

We for the first time developed photothermal nanodots by self-assembling peptide−porphyrin conjugates as PA and PTT agents. On account of the combinations of non-covalent interactions of peptides and porphyrins, these spherical PPP-NDs possess tunable diameter, high aqueous stability, excellent stability against dilution and irradiation, and relatively high light-to-heat conversion efficiency of 54.2%. The impressive efficiency facilitates the application of PPP-NDs for PA imaging and PTT. Extensive in vivo evaluations of PPP-NDs demonstrate their high biocompatibility to mice, accumulation in tumors, and efficient inhibition of the tumors. This study shows that stable photothermal nanodots can be constructed through rational design of self-assembling building blocks of peptides and light-absorbing molecules. As the stability in an aqueous solution and physiological medium, is compulsory and necessary for therapeutic applications, such a design of stable colloidal nanodots for a functional group such as porphyrin by

DOI: 10.1021/jacs.6b11382
J. Am. Chem. Soc. 2017, 139, 1921−1927

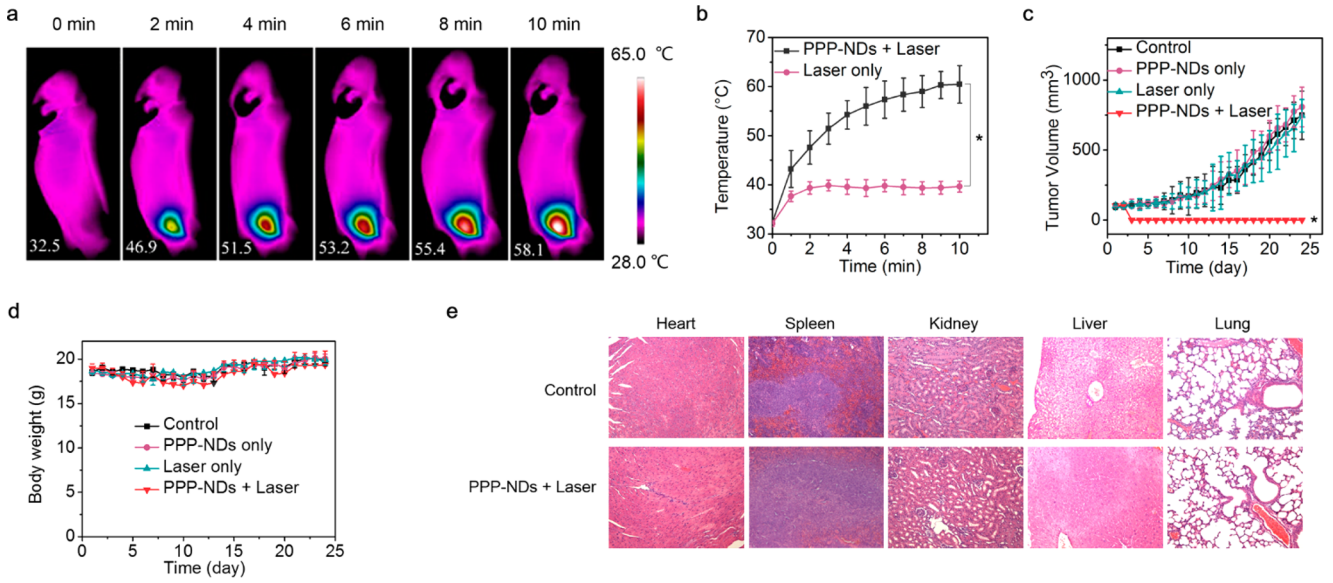

Figure 8. In vivo PTT. (a) IR thermal images of intravenous PPP-NDs injected mice under continuous irradiation. (b) Mean temperature of the tumor sites as a function of irradiation time ($n = 4$). *$P < 0.05$ (one-way ANOVA). (c) Tumor volume of the mice in different groups ($n = 4$). PPP-NDs were injected into mice for PTT (PPP-NDs + laser) in the first day, and they were then irradiated for 10 min at 24 h postinjection. *$P < 0.05$ (one-way ANOVA). (d) Body weight of the mice in different groups. (e) Hematoxylin and eosin (H&E)-stained histological section of heart, spleen, kidney, liver, and lung tissues obtained from mice of the control and PTT groups.

introducing a short peptide is highly valuable. This short peptide-tuned self-assembly strategy could be a powerful concept to construct efficient phototherapeutic nanomaterials together with various light-absorbing molecules, especially those possess near-infrared absorbance. More therapeutic effects, such as tumor targeting, can be integrated in the nanodots by tailoring the amino acid sequence of the peptide. Therefore, photothermal nanodots formed by self-assembly of small biomolecule combinations show flexibility, versatility, and adaptability for antitumor diagnosis and therapy. This will offer a new perspective in design of supramolecular therapeutic agents and may advance toward clinical translation and use of such biomaterials and nanomedicine.

■ ASSOCIATED CONTENT

Supporting Information

The Supporting Information is available free of charge on the ACS Publications website at DOI: 10.1021/jacs.6b11382.

Materials, methods, and supporting Figures S1−S19 (PDF)

■ AUTHOR INFORMATION

Corresponding Author

*yanxh@ipe.ac.cn

ORCID

Qianli Zou: 0000-0003-0464-4156

Xuehai Yan: 0000-0002-0890-0340

Author Contributions

#Q.Z. and M.A. contributed equally.

Notes

The authors declare no competing financial interest.

■ ACKNOWLEDGMENTS

We acknowledge financial support from the National Natural Science Foundation of China (Project Nos. 21522307, 21473208, 51403214, and 91434103), the Talent Fund of the Recruitment Program of Global Youth Experts, and the Chinese Academy of Sciences (Project No. QYZDB-SSW-JSC034). X.Y. is greatly indebted to Prof. Möhwald for his long-term support.

■ REFERENCES

(1) Lal, S.; Clare, S. E.; Halas, N. J. *Acc. Chem. Res.* **2008**, *41*, 1842.

(2) Huang, X. H.; El-Sayed, I. H.; Qian, W.; El-Sayed, M. A. *J. Am. Chem. Soc.* **2006**, *128*, 2115.

(3) Kim, J. W.; Galanzha, E. I.; Shashkov, E. V.; Moon, H. M.; Zharov, V. P. *Nat. Nanotechnol.* **2009**, *4*, 688.

(4) Wang, L. V. *Nat. Photonics* **2009**, *3*, 503.

(5) Wang, L. V.; Hu, S. *Science* **2012**, *335*, 1458.

(6) Taruttis, A.; Ntziachristos, V. *Nat. Photonics* **2015**, *9*, 219.

(7) Yang, J. M.; Favazza, C.; Chen, R. M.; Yao, J. J.; Cai, X.; Maslov, K.; Zhou, Q. F.; Shung, K. K.; Wang, L. H. V. *Nat. Med.* **2012**, *18*, 1297.

(8) Jaque, D.; Maestro, L. M.; del Rosal, B.; Haro-Gonzalez, P.; Benayas, A.; Plaza, J. L.; Rodriguez, E. M.; Sole, J. G. *Nanoscale* **2014**, *6*, 9494.

(9) Gao, L.; Fei, J. B.; Zhao, J.; Li, H.; Cui, Y.; Li, J. B. *ACS Nano* **2012**, *6*, 8030.

(10) Qin, C. C.; Fei, J. B.; Wang, A. H.; Yang, Y.; Li, J. B. *Nanoscale* **2015**, *7*, 20197.

(11) Dickerson, E. B.; Dreaden, E. C.; Huang, X. H.; El-Sayed, I. H.; Chu, H. H.; Pushpanketh, S.; McDonald, J. F.; El-Sayed, M. A. *Cancer Lett.* **2008**, *269*, 57.

(12) Yang, K.; Zhang, S. A.; Zhang, G. X.; Sun, X. M.; Lee, S. T.; Liu, Z. A. *Nano Lett.* **2010**, *10*, 3318.

(13) Robinson, J. T.; Tabakman, S. M.; Liang, Y. Y.; Wang, H. L.; Casalongue, H. S.; Vinh, D.; Dai, H. J. *J. Am. Chem. Soc.* **2011**, *133*, 6825.

(14) Sun, Z. B.; Xie, H. H.; Tang, S. Y.; Yu, X. F.; Guo, Z. N.; Shao, J. D.; Zhang, H.; Huang, H.; Wang, H. Y.; Chu, P. K. *Angew. Chem., Int. Ed.* **2015**, *54*, 11526.

(15) Tao, W.; Zhu, X.; Yu, X.; Zeng, X.; Xiao, Q.; Zhang, X.; Ji, X.; Wang, X.; Shi, J.; Zhang, H.; Mei, L. *Adv. Mater.* **2017**, *29*, 1603276.

(16) Pu, K. Y.; Shuhendler, A. J.; Jokerst, J. V.; Mei, J. G.; Gambhir, S. S.; Bao, Z. N.; Rao, J. H. *Nat. Nanotechnol.* **2014**, *9*, 233.

DOI: 10.1021/jacs.6b11382
J. Am. Chem. Soc. 2017, 139, 1921−1927

(17) Liu, Y. L.; Ai, K. L.; Liu, J. H.; Deng, M.; He, Y. Y.; Lu, L. H. *Adv. Mater.* **2013**, *25*, 1353.
(18) Lovell, J. F.; Jin, C. S.; Huynh, E.; Jin, H. L.; Kim, C.; Rubinstein, J. L.; Chan, W. C. W.; Cao, W. G.; Wang, L. V.; Zheng, G. *Nat. Mater.* **2011**, *10*, 324.
(19) Torchilin, V. P. *Nat. Rev. Drug Discovery* **2005**, *4*, 145.
(20) Cheng, J. X.; Xie, X. S. *Science* **2015**, *350*, aaa8870.
(21) Liu, K.; Xing, R. R.; Chen, C. J.; Shen, G. Z.; Yan, L. Y.; Zou, Q. L.; Ma, G. H.; Mohwald, H.; Yan, X. H. *Angew. Chem., Int. Ed.* **2015**, *54*, 500.
(22) Frederix, P. W. J. M.; Scott, G. G.; Abul-Haija, Y. M.; Kalafatovic, D.; Pappas, C. G.; Javid, N.; Hunt, N. T.; Ulijn, R. V.; Tuttle, T. *Nat. Chem.* **2015**, *7*, 30.
(23) Liu, K.; Xing, R. R.; Zou, Q. L.; Ma, G. H.; Möhwald, H.; Yan, X. H. *Angew. Chem., Int. Ed.* **2016**, *55*, 3036.
(24) Smits, F. C. M.; Buddingh, B. C.; van Eldijk, M. B.; van Hest, J. C. M. *Macromol. Biosci.* **2015**, *15*, 36.
(25) Wang, J.; Liu, K.; Xing, R. R.; Yan, X. H. *Chem. Soc. Rev.* **2016**, *45*, 5589.
(26) Adler-Abramovich, L.; Gazit, E. *Chem. Soc. Rev.* **2014**, *43*, 6881.
(27) Chen, C. J.; Liu, K.; Li, J. B.; Yan, X. H. *Adv. Colloid Interface Sci.* **2015**, *225*, 177.
(28) Ariga, K.; Ji, Q. M.; Mori, T.; Naito, M.; Yamauchi, Y.; Abe, H.; Hill, J. P. *Chem. Soc. Rev.* **2013**, *42*, 6322.
(29) Yan, X. H.; Zhu, P. L.; Li, J. B. *Chem. Soc. Rev.* **2010**, *39*, 1877.
(30) Reches, M.; Gazit, E. *Science* **2003**, *300*, 625.
(31) Li, Q.; Jia, Y.; Dai, L. R.; Yang, Y.; Li, J. B. *ACS Nano* **2015**, *9*, 2689.
(32) Ariga, K.; Li, J. B.; Fei, J. B.; Ji, Q. M.; Hill, J. P. *Adv. Mater.* **2016**, *28*, 1251.
(33) Tao, K.; Levin, A.; Adler-Abramovich, L.; Gazit, E. *Chem. Soc. Rev.* **2016**, *45*, 3935.
(34) Zou, Q. L.; Zhang, L.; Yan, X. H.; Wang, A. H.; Ma, G. H.; Li, J. B.; Mohwald, H.; Mann, S. *Angew. Chem., Int. Ed.* **2014**, *53*, 2366.
(35) Zou, Q. L.; Liu, K.; Abbas, M.; Yan, X. H. *Adv. Mater.* **2016**, *28*, 1031.
(36) Petros, R. A.; DeSimone, J. M. *Nat. Rev. Drug Discovery* **2010**, *9*, 615.
(37) Wurthner, F.; Kaiser, T. E.; Saha-Moeller, C. R. *Angew. Chem., Int. Ed.* **2011**, *50*, 3376.
(38) Lvov, Y. M.; Pattekari, P.; Zhang, X. C.; Torchilin, V. *Langmuir* **2011**, *27*, 1212.
(39) Fery-Forgues, S. *Nanoscale* **2013**, *5*, 8428.
(40) Liu, Y.; Kathan, K.; Saad, W.; Prud'homme, R. K. *Phys. Rev. Lett.* **2007**, *98*, 036102.
(41) Monteiro, C. J. P.; Pereira, M. M.; Azenha, M. E.; Burrows, H. D.; Serpa, C.; Arnaut, L. G.; Tapia, M. J.; Sarakha, M.; Wong-Wah-Chung, P.; Navaratnam, S. *Photoch. Photobio. Sci.* **2005**, *4*, 617.
(42) Ogilby, P. R. *Chem. Soc. Rev.* **2010**, *39*, 3181.
(43) Kuimova, M. K.; Yahioglu, G.; Ogilby, P. R. *J. Am. Chem. Soc.* **2009**, *131*, 332.
(44) Roper, D. K.; Ahn, W.; Hoepfner, M. *J. Phys. Chem. C* **2007**, *111*, 3636.
(45) Hessel, C. M.; Pattani, V. P.; Rasch, M.; Panthani, M. G.; Koo, B.; Tunnell, J. W.; Korgel, B. A. *Nano Lett.* **2011**, *11*, 2560.
(46) Xu, M. H.; Wang, L. H. V. *Rev. Sci. Instrum.* **2006**, *77*, 041101.
(47) De La Zerda, A.; Zavaleta, C.; Keren, S.; Vaithilingam, S.; Bodapati, S.; Liu, Z.; Levi, J.; Smith, B. R.; Ma, T. J.; Oralkan, O.; Cheng, Z.; Chen, X. Y.; Dai, H. J.; Khuri-Yakub, B. T.; Gambhir, S. S. *Nat. Nanotechnol.* **2008**, *3*, 557.
(48) Shao, J. D.; Xie, H. H.; Huang, H.; Li, Z. B.; Sun, Z. B.; Xu, Y. H.; Xiao, Q. L.; Yu, X. F.; Zhao, Y. T.; Zhang, H.; Wang, H. Y.; Chu, P. K. *Nat. Commun.* **2016**, *7*, 12967.

DOI: 10.1021/jacs.6b11382
J. Am. Chem. Soc. 2017, 139, 1921−1927